Food Research International 54 (2013) 1761–1772

Contents lists available at ScienceDirect

Food Research International

journal homepage: www.elsevier.com/locate/foodres

Electrospinning of ethyl cellulose fibres with glass and steel needle configurations

Bilal Ahmad [a], Simeon Stoyanov [b], Eddie Pelan [b], Eleanor Stride [a,c], Mohan Edirisinghe [a,*]

[a] Department of Mechanical Engineering, UCL, Torrington Place, London WC1E7JE, UK
[b] Unilever Research, Olivier van Noortlaan 120, 3130AC Vlaardingen, The Netherlands
[c] Institute of Biomedical Engineering, Department of Engineering Science, University of Oxford, Old Road Campus, Headington, Oxford OX3 7DQ, UK

ARTICLE INFO

Article history:
Received 14 February 2013
Accepted 16 September 2013

Keywords:
Electrospinning
Glass needle
Steel needle
Fibre aspect ratio
Ethyl cellulose

ABSTRACT

A novel device to produce ethyl cellulose fibres, an important biomaterial in modern food processing, using a glass needle in a modified electrospinning setup has been investigated. The effect of applied voltage on the fibre aspect ratio was analysed during electrospinning with a metallic (stainless steel) needle and then compared with that obtained with a glass–steel needle combination. A distinct difference in fibre diameter was observed between the two needle setups for the same processing conditions. A detailed quantitative study of the fibre length and diameter with respect to applied voltage was also carried out in order to determine any relationship between the needle material and the resulting electrospun fibres. There was an increase in fibre diameter in the case of steel–steel needle electrospinning with increasing applied voltage while a decrease in fibre diameter was observed with glass–steel needle electrospinning for the same voltage.

1. Introduction

A major focus of public health strategies aimed at preventing early onset of chronic diseases such as cardiovascular disease, obesity and gastrointestinal (GI) disorders is diet. The highly complex relationship between food and health is still poorly understood but recent research advances in various different disciplines of food and health sciences have improved its understanding substantially (Liu, 2003). The increasing consumer health consciousness and the subsequent growing demand for healthy foods have encouraged innovation in product design and development of functional food products in the food industry worldwide.

Generally, a food can be regarded as functional if, in addition to its inherent nutritional effects, it can demonstrate an ability to either bring about a beneficial effect to a target function inside the body or prevent the onset and/or risk of disease or both (Lopez-Rubio, Gavara, & Lagaron, 2006).

Therefore, development of functional foods is a great opportunity to improve the quality of foods available to consumer's demand and need for healthy nutrition. At present, the industrial demand for technologies that can produce novel functional food structures is strong and growing. New technologies such as micro- and nano-encapsulation provide promising prospects (e.g. controlled release of nutrients) for improved food functionality (Jimenez, Garcia, & Beristain, 2004). In addition, structures of different morphologies, including solid and hollow fibres, microbubbles, encapsulated particles and foams have been prepared using a number of different materials and methods. Some of these methods include: self-assembly, microfluidics, and electrospinning (Ahmad, Stride, & Edirisinghe, 2012; Sill & von Recum, 2008; Zhang, 2003). However, development of these techniques is still in its relative research infancy with respect to their application in the food industry and far from being considered as fully optimised commercial food processing methods. Thus, the scope of the present work is to provide more understanding of one of the aforementioned techniques, in this case electrospinning, by improving its utility in constructing fibrous structures out of food compatible biomaterials. The potential of using electrospinning in food processing could be profound. For example, electrospinning can be used to create synthetic dietary fibres that naturally consist of the structural and storage polysaccharides (such as cellulose) and lignin in plants. Dietary fibre has demonstrated ample benefits in health maintenance and disease prevention and as an important component of medical nutrition (Kris-Etherton et al., 2002). The daily recommended intake of dietary fibre for adults and children is not being met due to the low consumption of natural sources of dietary fibre such as vegetables, fruits and high grain products. With electrospinning, the quantity of fibre content can be varied either to increase or decrease the recommended intake. In addition, other vital components of healthy nutrition such as vitamins can also be added to these synthetic fibres.

For producing fibrous structures for biotechnology applications, electrospinning has emerged as a potentially attractive option due to its simplicity and relatively inexpensive setup. In this technique, a polymer solution flows out of a nozzle and is drawn towards a grounded collector under the influence of an applied electric field to form a non-woven mesh of fibres. Fibres can be easily electrospun with diameters

* Corresponding author. Tel.: +44 2076793942; fax: +44 2073880180.
E-mail address: m.edirisinghe@ucl.ac.uk (M. Edirisinghe).

0963-9969/$ – see front matter © 2013 Elsevier Ltd. All rights reserved.
http://dx.doi.org/10.1016/j.foodres.2013.09.021

of the order of 100 nm provided the solution and processing parameters such as applied voltage and flow rate are optimised. At this scale, some very important characteristics are obtained such as high surface area to volume ratio which is desirable in a range of different applications such as scaffolds for tissue engineering and fibre reinforced composite products (Li & Xia, 2004).

In recent years, several modifications have been made to the basic electrospinning process in order to bring it in line with the high production standards characteristic of commercial spinning techniques as well as to improve the functionality of the resulting structures. At present, single-needle systems for electrospinning have been used extensively but the low material throughput in spinning has limited the industrial use. To meet high liquid throughput requirements, several multi-jet schemes have been tested in the recent past (Dosunmu, Chase, Kataphinan, & Reneker, 2006; Ying et al., 2006). The main drawback of these schemes is the deterioration of the local electric field at the needle tip due to the presence of other needles in the arrangement (Ying et al., 2006). This results in non-uniform fibre formation and the requirement for higher voltages for jet initiation (Dosunmu et al., 2006). Also, there exists a debate with respect to the electrospinning process as some researchers have observed that a higher electric field leads to greater stretching (drawing stress) of the jet, resulting in thinner fibres (Angammana & Jayaram, 2011; Lee et al., 2004; Mo, Xu, Kotaki, & Ramakrishna, 2004; Shin, Hohman, Brenner, & Rutledge, 2001).

One of the modifications made to the electrospinning setup is the use of co-axial needles, in which a concentric spinneret can accommodate two different liquids which are drawn to generate fibres in a core-sheath configuration; this modification has been regarded as one of the most important breakthroughs in electrospinning (Dzenis, 2004). Co-axial electrospinning has been applied in various applications specifically to control fibre morphology (including fibre aspect ratio which is essentially the ratio between diameter and length but sometimes expressed as length/diameter) (Yarin, 2011), to encapsulate drugs or biological agents fibres (Zhang et al., 2009), to prepare nanofibres from materials that lack filament-forming properties (Yu, Fridrikh, & Rutledge, 2004), and recently, to encapsulate microbubbles in fibres (Ahmad, Gunduz, et al., 2012).

In this work, we present a new method to electrospin fibres using two needles, a metallic outer needle and a glass inner needle, which are concentrically aligned just as they are in a co-axial electrospinning setup. Unlike co-axial electrospinning, however, we perfused only the inner needle of the setup while the outer metallic needle acted as an electrical conduit to create the electric field necessary for electrospinning. A detailed comparison between glass–steel needle and steel–steel needle setups was then made in order to demonstrate the utility, if any, of the glass–steel needle setup over the steel–steel needle setup to generate fibres. An analysis into the difference in electrical field generation in both needle setups was also carried out.

Ethyl cellulose (EC) was chosen as the primary polymer to illustrate this method due to its long history in fibre manufacturing (Cuculo, Aminuddin, & Frey, 2000), abundant availability, biocompatibility and its increasing application in the food engineering industry (Ahmad, Gunduz, et al., 2012). Ethyl cellulose is commonly used as an emulsifier, thickening agent and dietary fibre in food products primarily due to its cost effectiveness. In addition, these properties also make EC useful in a wide range of other biotechnology fields such as biomedical applications and filtration (Kim, Kim, Kang, Marquez, & Joo, 2006). Other varieties of cellulose are also gaining interest in the food sector. For example, recently, bacterial cellulose (BC), a nano-scale polyglucose, was investigated for its fine network and biocompatibility (Yan et al., 2008). BC is superior to plant cellulose owing to its purity and nano-morphology in combination with a variety of properties such as high water holding capacity, large surface area, and elasticity. The material is expected to play a major role as a food additive, as a scaffold in tissue engineering, in food packaging, and in the preparation of composite materials (Chang, Chen, Lin, & Chen, 2012).

The engineering process elucidated in this paper is generic and is applicable to other polymer materials suitable for fibre generation and the understanding behind it should significantly add to the existing knowledge base of fibre generation methods. In addition, being able to electrospin polysaccharides in a food-grade way opens a new route towards nutritionally appealing dietary fibres. The subsequent steps in the line towards its industrial application are the control over fibre uniformity and upscaling of the process to meet the stringent demands of the food industry.

2. Experimental section

2.1. Materials

To electrospin ethyl cellulose (M_w ~ 100,000 Sigma-Aldrich, Poole, UK), seven solutions of it were prepared with varying concentrations, ranging from 5 wt.% to 35 wt.%. The ethyl cellulose powder was dissolved in 10 ml of a binary solvent system of ethanol (BDH Laboratory Supplies, Poole, UK) and de-ionised water (80:20) and stirred for 2 h at the ambient temperature (~24 °C). All solutions were prepared by simple mixing in the same way and in the same volume ratio for this study.

2.2. Characterisation

The physical properties of the liquids: viscosity, surface tension and electrical conductivity were measured at the ambient temperature (~24 °C) using a viscometer (Brookfield DV-III Ultra, Labsource, Manchester, UK) and RheoCalc V3 software, a Kruss K9 tensiometer (Kruss Surface Science Centre, Bristol, UK) and a HANNA HI 8733 conductivity meter (CamLab Ltd, Cambridge, UK), respectively. Each device was calibrated using ethanol prior to the measurements.

2.3. Needle type and setup

A borosilicate glass needle (composition: 70 wt.% silica, 10 wt.% boron oxide, 8 wt.% sodium oxide, 8 wt.% potassium oxide, 3 wt.% aluminium oxide and 1 wt.% calcium oxide, Linari Engineering, Pisa, Italy) of internal diameter 686 μm was used. The two steel needles used, were of internal diameters 686 μm and 810 μm (Stanley Engineering, Birmingham, UK), respectively (Fig. 1a).

2.3.1. Steel–steel needle setup

This needle setup is essentially very similar to that used in co-axial electrospinning but, here, the outer needle was only used as a conduit to create the electrical field for the liquid that is perfused through the inner needle and the grounded collector, rather than being used as a channel to deliver the second liquid.

To keep the needle comparison as consistent as possible, a 686 μm diameter steel needle was used to electrospin fibres; the needle was concentrically aligned with the external steel (810 μm) needle (Fig. 1b). The gap between both steel needles was approximately 60 μm. The cross-section of the needle setup is also shown diagrammatically in Fig. 1b.

2.3.2. Glass–steel needle setup

The glass–steel needle setup was similar in geometry to the steel–steel setup except that the glass needle was inserted into the steel outer needle and held in place firmly with plasticine. Utmost care was taken to not let the glass needle touch the steel needle internally. The gap between the glass and steel needle was again, approximately 120 μm.

2.4. Fibre electrospinning

Two separate but identical sets of experiments were carried out using both types of needle setups on all the ethyl cellulose solutions

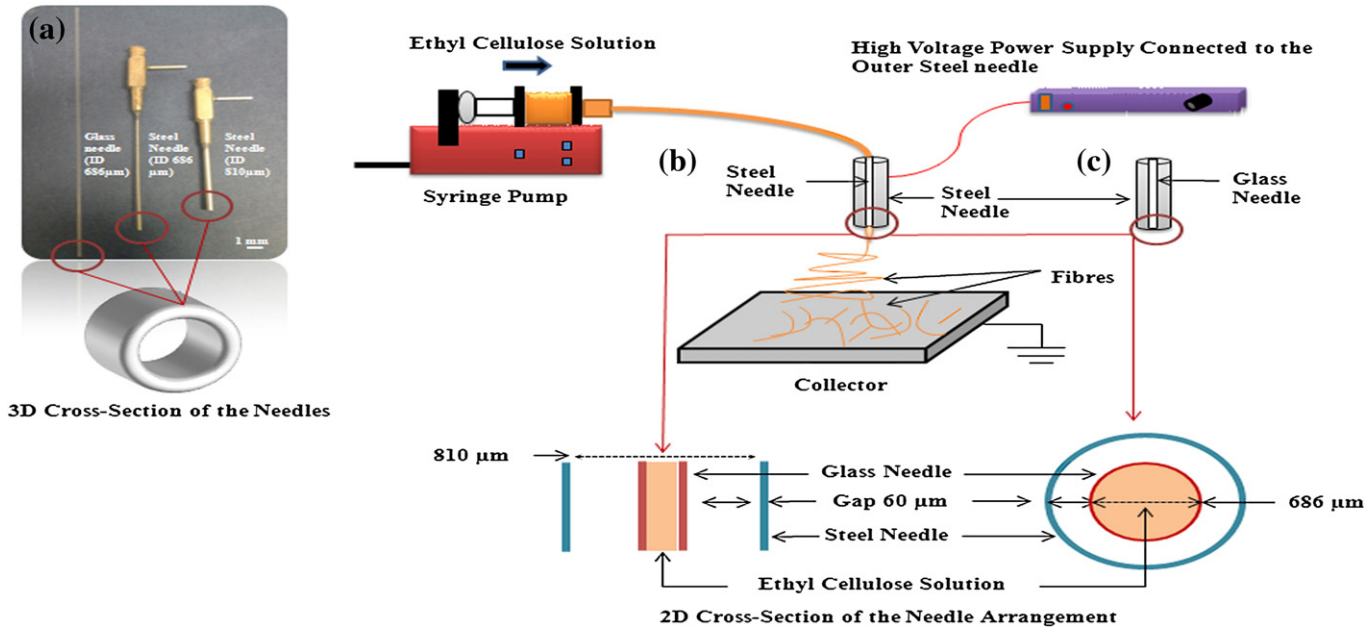

Fig. 1. (a) Photograph of the glass needle (left) and steel needles (middle and right) used in this study (ID refers to internal diameter), (b) and (c) schematic diagram of the steel–steel needle and glass–steel needle setups, respectively, used to electrospin the ethyl cellulose fibres. The 2D cross-section shows that for both needle setups the gap, between the co-axially aligned needles, was the same. Internal diameter of the needles is (from left to right), 686 µm, 686 µm and 810 µm.

(5–35 wt.%). Ethyl cellulose solution was fed into the needles through a silicone tube (ID ~ 1 mm, VWR International Ltd, East Grinstead, UK). In both cases, i.e. glass–steel needle and steel–steel needle electrospinning, the voltage was applied between the outer steel needle and a grounded collector which was placed 100 mm away from the needle exit throughout the study. A high voltage power supply (FC 120W, Glassman Europe Limited, Bramley, UK) was used and the liquid flow rate was controlled via a 10 ml plastic syringe mounted on a syringe pump (Harvard, PHD 4400, Harvard Apparatus, Eden bridge, UK). A flow rate of 40 µl/min was used throughout the study. The applied voltage was increased in small increments to create the electric field strength needed to spin fibres. Fibre samples were collected on glass slides for analysis. To ensure reproducibility, several samples of fibres were produced using both needle setups at different times. All the numerical results shown represent the average of 10 repeats.

Fibres obtained from both needle setups were collected on dry glass slides and observed under the optical microscope (Zeiss Axiotech) fitted with a Q-imaging Micropublisher 3-3RTV camera before images were taken. The fibre samples were then dried in air for 1 day, sputter coated with gold for 180 s and then analysed under the scanning electron microscope with an accelerating voltage of 10 kV.

3. Results and discussion

3.1. Solution concentration

The optimum ethyl cellulose concentration to form fibres with little or no beading was found to be 20 wt.%. Solutions of concentration less than 20% resulted in no fibres as the viscosities of the solutions were too low and solutions over 20% resulted in thick fibres with excessive beading and in the case of 35% concentration, needles were consistently being blocked.

Another trend observed during this study was the increase in electrical conductivity with increasing concentration of ethyl cellulose in the prepared solutions (Table 1). Higher conductivity solutions favour jet formation and fibre spinning when subjected to a high applied voltage (Dzenis, 2004). This results in the forces involved in the electrospinning process, notably, the Coulomb force between the charges on the jet surface, to cause a significant drop in the diameter of the electrospun fibres (Reneker, Yarin, Fong, & Koombhongse, 2000). Another similar study (Kim, Lee, & Kim, 2005) also confirmed this, explaining that with increased electrical conductivity, the jet carries more charge resulting in more electrostatic repulsion at the surface of the electrospinning jet which leads to greater stretching (a higher drawing stress) of the solution.

3.2. Steel–steel needle fibre generation

Once the droplet of ethyl cellulose solution exited the needle tip, voltage was applied to create an electric field between the needle tip and the grounded collector to start the spinning process. Initially, the applied voltage was increased in small increments until fibres started to appear. A high speed camera (Phantom V7.1 camera, maximum resolution of 800 × 600 pixels at up to 4800 fps giving 1.2 s of recording time, Vision Research, Bedford, UK) was used to capture images of the electrospinning process for both needle setups. It was possible to see the evolution of the liquid droplet from the needle with increasing voltage, and from the formation of a cone to the generation of multiple fibres. In the conventional view of electrospinning, electrostatic charging of the fluid at the tip of the needle results in the formation of the well-known Taylor cone, from the apex of which a single fluid whipping jet is ejected. As the jet accelerates and thins in the electric field, radial

Table 1
Properties of ethyl cellulose solutions used in this investigation.

Ethyl cellulose solution concentration	Viscosity (mPa s)	Surface tension (mN/m)	Electrical conductivity (S/m × 10^{-4})
5%	23 (±5)	25 (±1)	47 (±0.5)
10%	100 (±9)	29 (±1)	61 (±0.6)
15%	363 (±11)	36 (±2)	68 (±0.6)
20%	1230 (±17)	54 (±3)	84 (±1.0)
25%	3692 (±28)	*	80 (±4.0)
30%	11,629 (±55)	*	800 (±8.0)
35%	14,600 (±72)	*	1100 (±11.0)

* indicates that accurate surface tension measurements with plate method were not possible due to the high viscosity of solution.

charge repulsions results in splitting of the primary jet into multiple filaments, in a process known as splaying (Jaworek & Krupa, 1992).

In the case of the steel–steel needle electrospinning, as shown in Fig. 2, a steady-bending mode (Hohman, Shin, Rutledge, & Brenner, 2001; Jaworek & Krupa, 1992) at the tip of the needle was observed when the ethyl cellulose solution escaped the steel needle. This is the most widely reported mode of electrospinning in the literature. A straight jet is steadily ejected from the tip of the cone. At a certain distance from the tip of the cone, the jet thins and starts to bend. The length of the straight jet and the angle of the jet envelope always remain constant. As the bending jet moves towards the collector, the second bending instability takes place. The jet diameter in this mode is uniform (Ting, Li, Chen, Tian, & Yin, 2012).

Short fibres (length < 5 μm) started to appear once the applied voltage was increased to 5 kV (Fig. 3a). The fibres became longer (length > 8 μm) as the voltage was increased past 10 kV (Fig. 3b, c). The diameter of the fibres increased (from 1.5 μm to 2 μm) with increasing voltage (Fig. 3d). It is also clear from the optical images that increasing voltage resulted in the formation of beads on the fibres with their apparent numbers increasing at higher voltages (15 kV). The scanning electron micrographs of the same fibre samples also confirmed the change in fibre length and diameter with an increase in voltage as well as the appearance of beads (Fig. 4).

3.3. Glass–steel needle fibre generation

The electrospinning of ethyl cellulose fibres was also carried out with glass–steel needles to compare the fibre generation from both methods. The solution concentration of ethyl cellulose and the collection distance were kept the same. The high-speed camera images (Fig. 5) for this setup show a different cone and jet evolution known as the rotating bend mode (Ting et al., 2012). This type of mode normally results from changes in the electrospinning parameters. For example, when the electric potential increases, the straight jet deviates from its original position and rotates at an angle (bend) from the cone which itself is slightly skewed (Fig. 5h). This change was expected as there would be a change in the character of the electrical field with the introduction of an electrically non-conductive needle component (glass) to the electrospinning setup. This mode also occurs when there is a build-up of positive charge within the polymer solution. Since with the glass needle the solution was surrounded by a non-conductive wall, only after exiting the glass needle could the solution experience such a charge build-up, which is attracted to the steel outer needle. The cone being skewed and slightly non-perpendicular to the grounded collector was the result of the force from that charge build-up that draws the droplet coming out from the glass needle to the grounded electrode (Ramakrishna, Fujihara, Teo, & Ma, 2005, chap. 3).

Fibres started to emerge at 5 kV, with the glass needle setup, though variable in their aspect ratio (Fig. 6a), but continuous spinning was optimal at 14 kV. There was no fibre generation below 5 kV. The fibres analysed under the optical microscope on glass slides showed the effect of increasing voltage on fibre diameter. Fibre length was short (<10 μm) at low voltages (5 kV) and there were traces of beads (Fig. 6b, c) but far fewer than in the fibres produced from the steel–steel needle setup. The beading started to disappear once the voltage was increased to >14 kV (Fig. 6d). Upon closer examination, the scanning electron micrographs also confirmed the change in fibre morphology with changing voltage (Fig. 7), with fibres getting longer (<15 μm) with increasing voltage. The diameters of the fibres, however, showed a different trend from those seen in the steel–steel needle setup with larger diameters at low voltages (>2.5 μm) and smaller diameters (<1.5 μm) at higher voltages (15 kV).

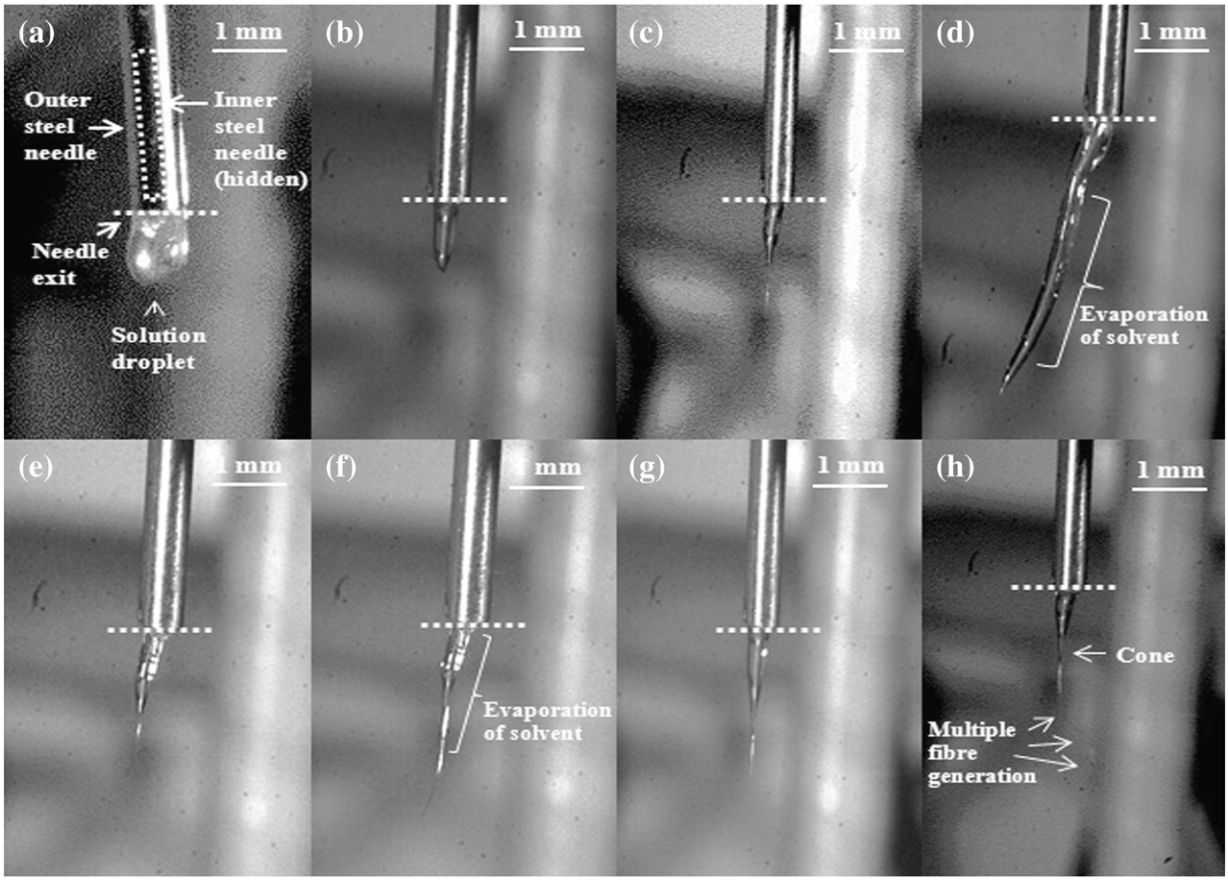

Fig. 2. High speed camera images of steel–steel needle setup electrospinning at (a) 0 kV, (b) 3 kV, (c) 5 kV, (d) 8 kV, (e)10 kV, (f) 12 kV, (g) 14 kV and (h) 15 kV.

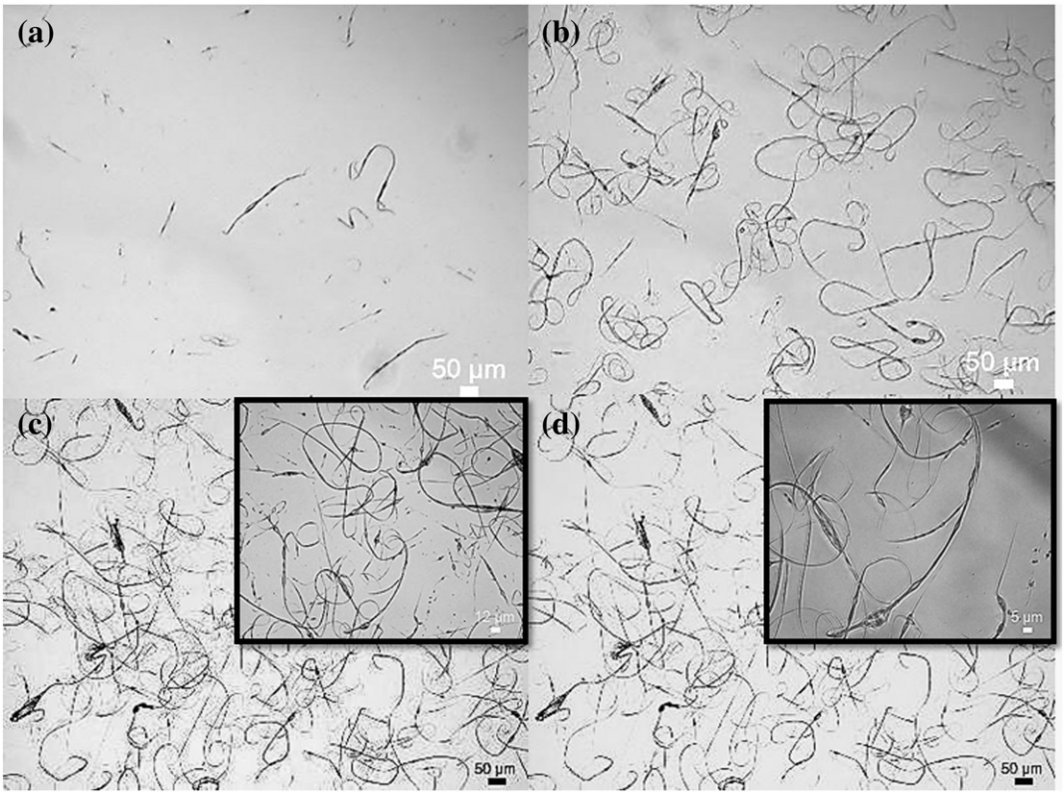

Fig. 3. Optical micrographs of ethyl cellulose fibres electrospun via the steel–steel needle setup at (a) 5 kV, (b) 7 kV, (c) 10 kV and (d) 15 kV taken at ×5 magnification. The image inserts in (c) and (d) are taken at ×20 and ×50 magnifications, respectively. The scale bar on the inserts reads 12 μm and 5 μm, respectively.

3.4. Applied voltage and fibre diameter

A quantitative analysis was carried out on the length and diameter of fibres produced by both needle setups. For each needle type, 200 measurements of length and diameter were carried out using the Image J tool (public domain open source image processing software available online). Measurements were made for three voltages, 5, 10 and 15 kV to maintain a consistent comparison between the glass and

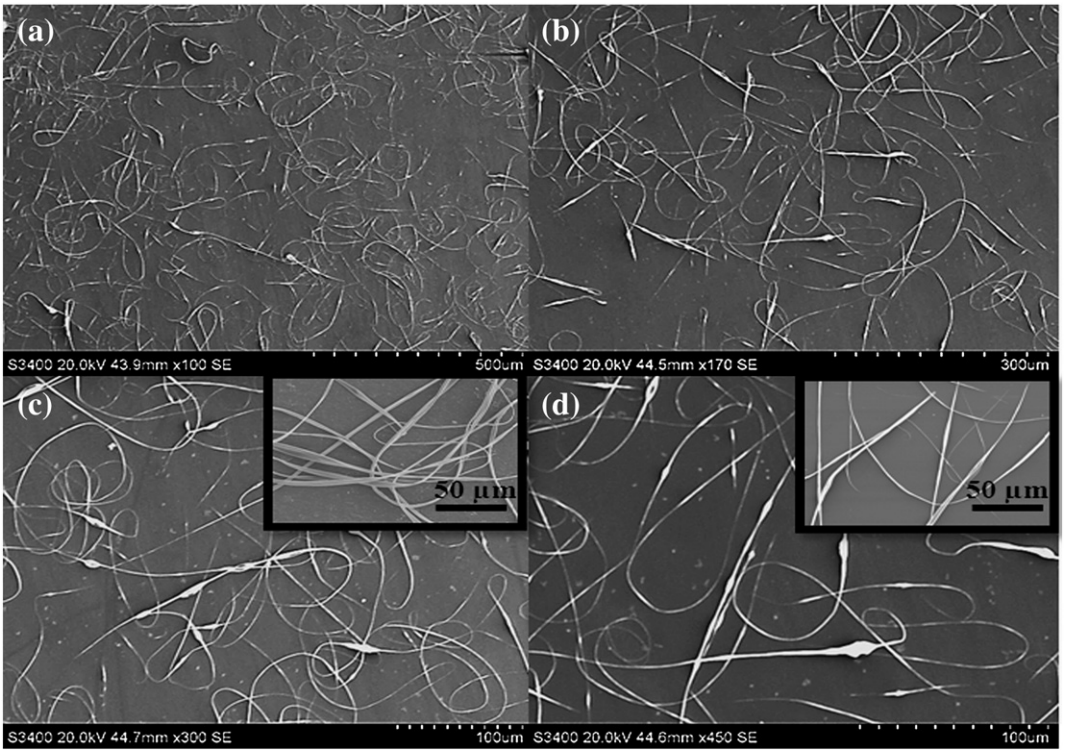

Fig. 4. Scanning electron micrographs of ethyl cellulose fibre electrospun via the steel–steel needle setup showing the change in fibre diameter with increasing voltage. (a) 5 kV, (b) 7 kV, (c) 10 kV and (d) 15 kV.

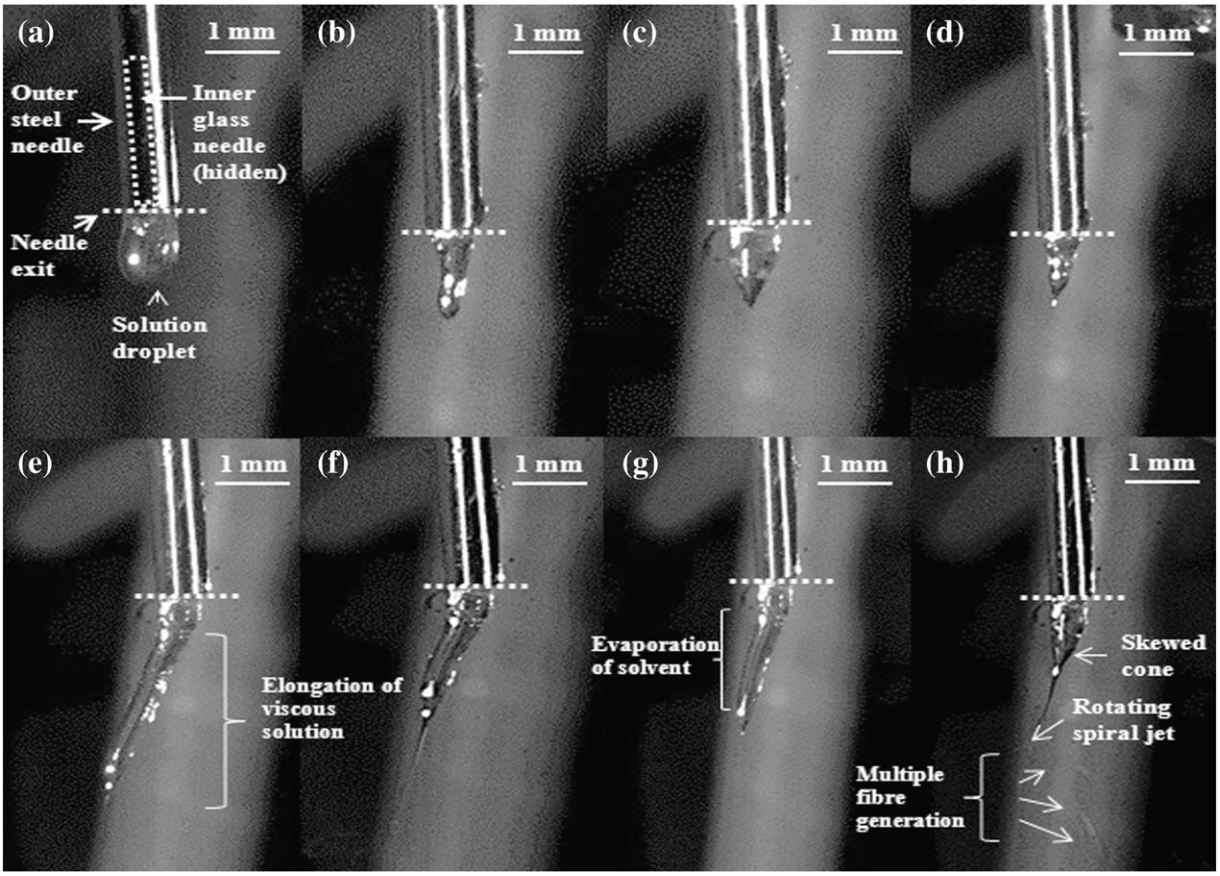

Fig. 5. High speed camera images of glass–steel needle electrospinning at (a) 0 kV, (b) 2 kV, (c) 4 kV, (d) 6 kV, (e) 8 kV, (f) 10 kV, (g) 12 kV and (h) 15 kV.

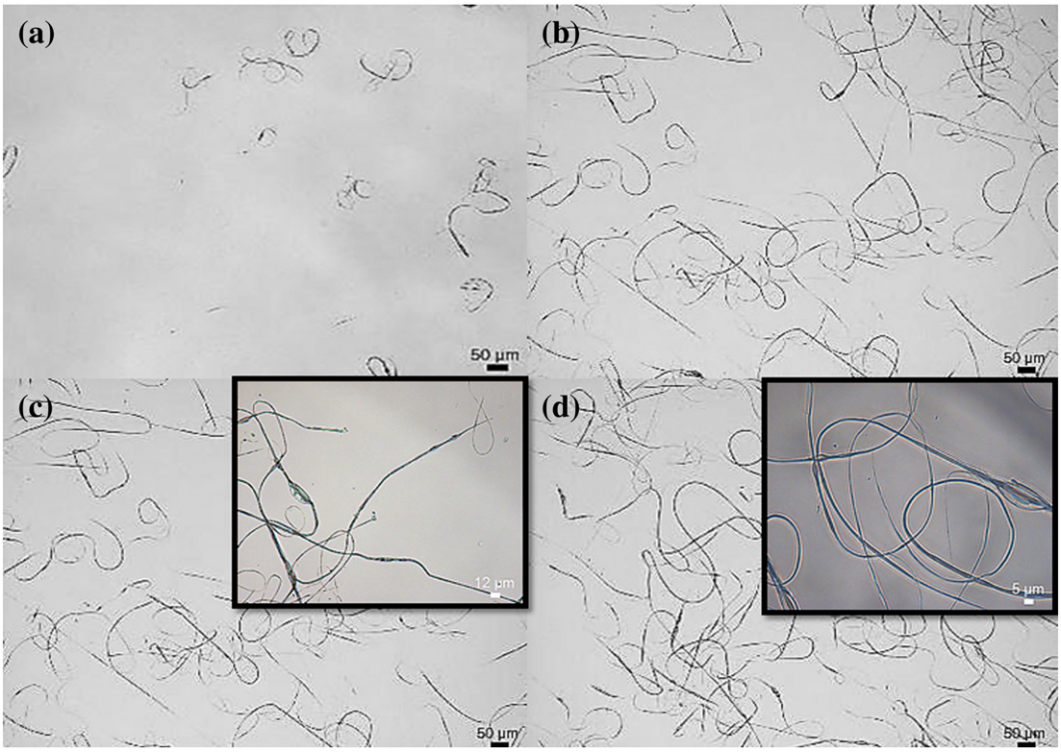

Fig. 6. Optical micrographs of ethyl cellulose fibres electrospun via the glass–steel needle setup at (a) 5 kV, (b) 7 kV, (c) 10 kV and (d) 15 kV taken at ×5 magnification. The image inserts in (c) and (d) are taken at ×20 and ×50 magnifications, respectively. The scale bar on the inserts reads 12 μm and 5 μm, respectively.

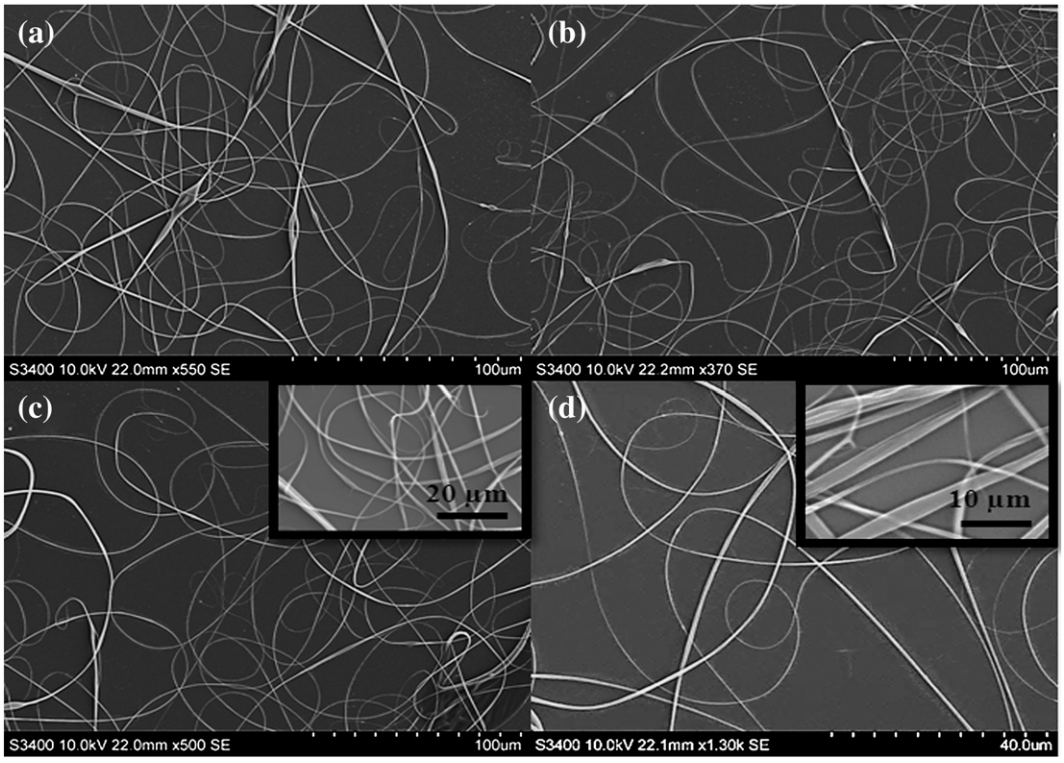

Fig. 7. Scanning electron micrographs of ethyl cellulose fibre electrospun via the glass–steel needle setup showing the change in fibre diameter with increasing voltage (a) 5 kV, (b) 7 kV, (c) 10 kV and (d) 15 kV.

steel needle electrospinning setups, respectively. Fig. 8 shows the fraction of fibres produced with different diameters as the applied voltage was increased for the steel–steel needle setup. More fibres were produced as the voltage increased. In addition, the average fibre diameter also increased with values of 1.2 μm, 1.3 μm and 1.9 μm, respectively, at the three different voltages. The increase in fibre diameter can be attributed to the presence of beads on the fibres and their fusion leading to the formation of thicker fibres as the voltage was increased (Jaworek & Krupa, 1992).

In the case of the glass–steel needle setup, the fraction of fibres with smaller diameters increased with increasing voltage (Fig. 9). Thus, the average fibre diameter also decreased with values of 1.7 μm, 1.6 μm, and 1.2 μm, for 5, 10 and 15 kV, respectively. The fibre length at 10 kV decreased with increasing fibre diameter but the pattern was reversed at 15 kV. Since it was not clearly conclusive whether the fibre length had a limiting effect on the diameter (or vice-versa) the aspect ratio (length: diameter) of the fibres was calculated and plotted against the applied voltage (Fig. 10.). It can be seen that for both needle setups, the average fibre aspect ratio increased with voltage at first (10 kV) for the steel–steel needle but was constant for the glass–steel needle and then both decreased. The drop in aspect ratio from 10 kV to 15 kV for both needle setups was high. The steel–steel needle setup exhibited a 58% (±2.5) decrease in aspect ratio whereas the glass–steel needle setup was lower at 42% (±2.5). It is also important to note that at 10 kV, the aspect ratio, for both setups was very similar and that a difference was only present when the voltage was at 5 kV or at 15 kV. This indicates that 10 kV was the critical voltage for electrospinning ethyl cellulose fibres as the difference in aspect ratio for fibres from both needle setups was small at this voltage and a decrease or an increase in voltage from this value resulted in a larger difference in fibre aspect ratio (Fig. 10).

The variables investigated in this study — polymer concentration, applied voltage (and consequently electric field between needle tip and grounded collector) and needle material had significant effects on the resulting fibre aspect ratio. Furthermore, it can also be concluded from the results that understanding behind the above mentioned factors can be combined with the knowledge of other forces acting on the fibres after contact with the grounded collector, such as adhesion to the collector, the weight of the fibre, electrostatic attraction to the ground and repulsion from neighbouring fibres, to further improve the control over the fibre aspect ratio during electrospinning. With a lack of literature available on non-metallic needle electrospinning, the decrease in fibre diameter with the glass–steel needle setup could be further explored by understanding the electric field generation when needles of different electrical conductivities are employed. One of the ways to understand this is to look at the dielectric properties of the needles involved. Metals naturally are not good dielectric materials and since borosilicate glass has a relatively high dielectric strength (10 kV/mm at 20 °C), the reduction in fibre diameter in the case of the latter can possibly be explained as some studies have shown that a solution with a greater dielectric property reduces the bead formation and the diameter of the resulting electrospun fibre (Ting et al., 2012).

3.5. Electric field measurement

The electrospinning process is highly dependent on the electric field, particularly the local field at the needle tip, which determines the nature of the electrospinning process and the morphology of the fibres. In a recent study (Angammana & Jayaram, 2011), a computer simulation was carried out to calculate the local electric field at the needle tip during the electrospinning process. Several assumptions were made during this study in order to elucidate the change in electric field when multiple metallic needles are employed during electrospinning and how the field deteriorates with increasing number of these needles. This method does not take into account numerous considerations such as surface tension force, gravity force, and air drag force due to air friction, which are essential to fully understand the electric field generation during the electrospinning process (Kim et al., 2005).

In our study, we attempted to establish an empirical relationship between electric field and fibre diameter for both needle setups. The

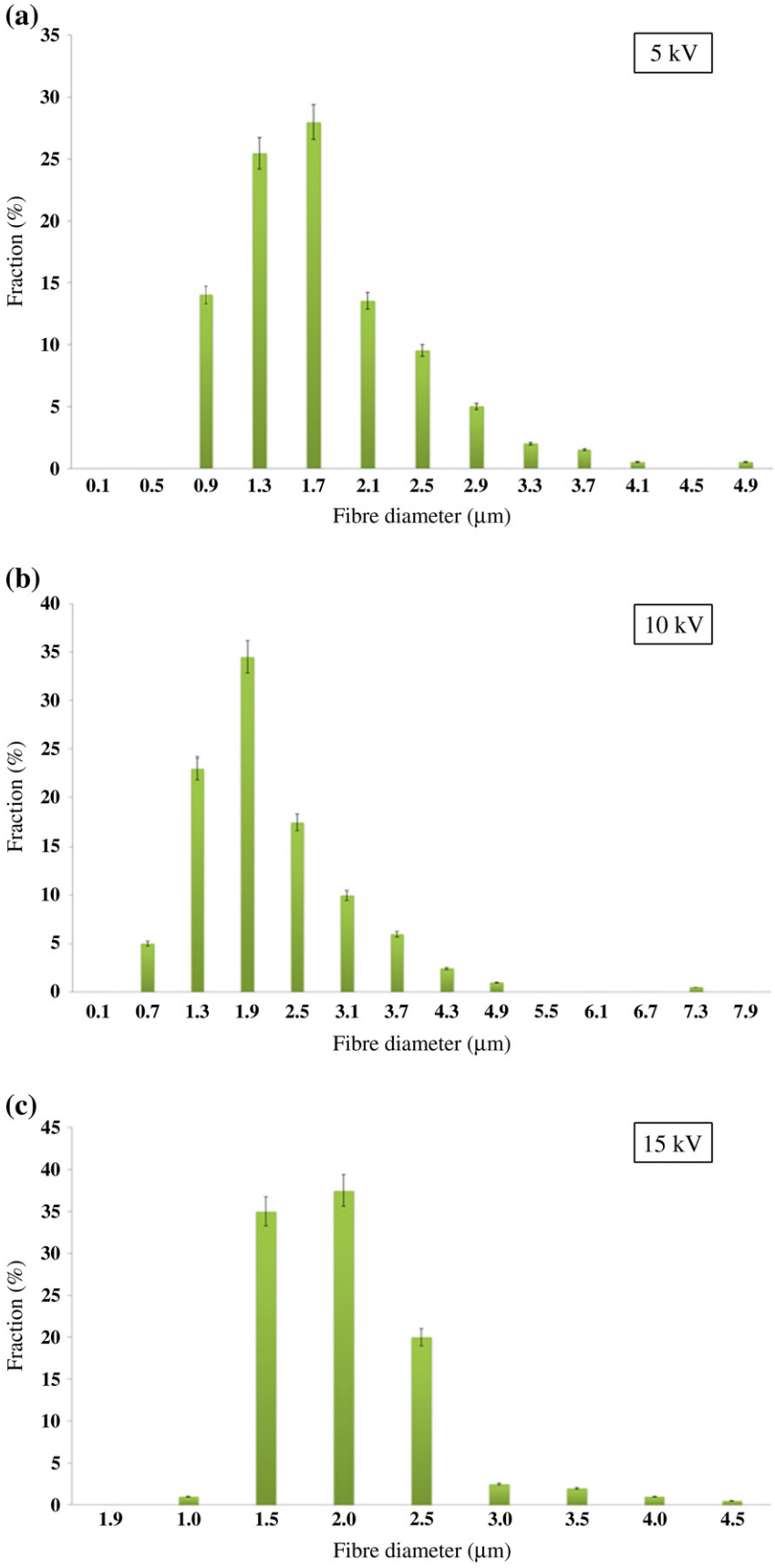

Fig. 8. The fraction of fibres produced by the steel–steel needle setup with different diameters in this study at (a) 5 kV, (b) 10 kV and (c) 15 kV, respectively. A total of 200 measurements of fibre diameter were made for each of the three applied voltages.

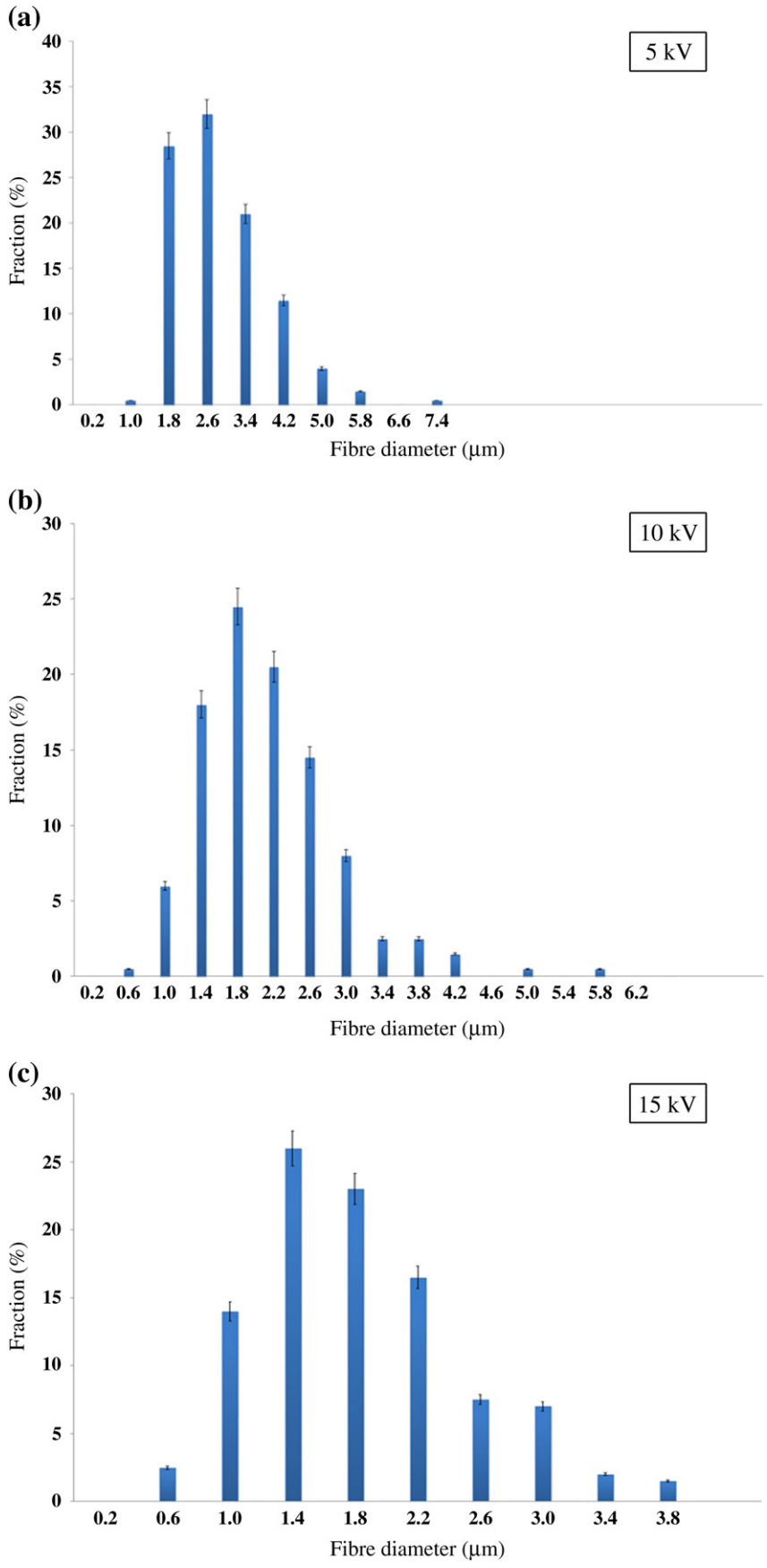

Fig. 9. The fraction of fibres produced by glass–steel needle setup with different diameters in this study at (a) 5 kV, (b) 10 kV and (c) 15 kV, respectively. A total of 200 measurements of fibre diameter were made for each of the three applied voltages.

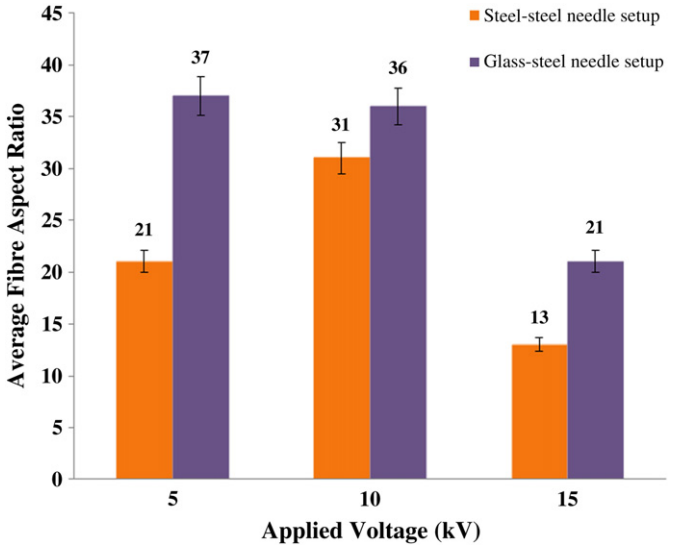

Fig. 10. The effect of applied voltage on average aspect ratio for both needle setups used in this study. Each column for each setup represents a total of 200 measurements of fibre length and diameter, respectively.

electric field was not measured at the needle tip but instead between the needle and the collector. For that, the difference in voltage between the needle tip and the grounded collector had to be measured first during the electrospinning process for both the glass–steel and steel–steel needle setups. A voltmeter (UNI-T UT58A, Rotherham, UK) was used to measure the voltage across the whole length (110 mm) of the grounded collector, which was placed 100 mm away from the needle tip (Fig. 11a). The values were recorded for each of the three applied voltages 5, 10 and 15 kV and an average of ten readings per voltage was taken using the voltmeter. For steel–steel needle setup they were 12 V (±2.0), 24 V (±1.1) and 84 V (±4.0), respectively. In comparison, the glass–steel needle setup recorded higher values for each of the applied voltages: 23 V (±1.0), 52 V (±3.2) and 98 V (±2.4), respectively. However, these values are invalid for a number of reasons. The voltage picked up on the voltmeter could be from the coronal discharge (Tang & Gomez, 1995) taking place within the solution and in the needle; or it could be the positively charged fibres reaching the grounded collector or the ions created in the air between the needle and the collector. In all these cases, the readings could register on the voltmeter just as the charge is dissipated to the grounded collector and there is no way to confirm which value of the applied voltage was recorded. Hence, calculating the electric field from these values would be incorrect.

Furthermore, if the measured voltages were not used then the change in voltage from the needle tip to the grounded collector can be taken as the difference between applied voltage and the voltage at the collector (which would be zero since its grounded) divided by the distance between the needle tip and the grounded collector. This was done by using the parallel plate method (Fig. 11b). In this method, a uniform field was assumed which essentially means that the electric field is completely perpendicular to the grounded collector. The conducting needle and the collector were treated as infinite planes (neglecting fringing) with the presumption that the plates were at equilibrium with zero electric field inside the conducting electrode (i.e. outer steel needle). This means that the electric field was taken to be constant at every point. Ignoring the edge effects such as needle geometry, the equation for the magnitude of the electric field (E) was simplified to:

$$V_i - V_f = -Ed \quad (1)$$

where, V_i is the voltage generated by the power supply, V_f is the voltage measured at the grounded collector by the voltmeter and d is the distance between the needle tip and the grounded collector. Using Eq. (1), the electric field values for the three applied voltages, i.e. 5, 10

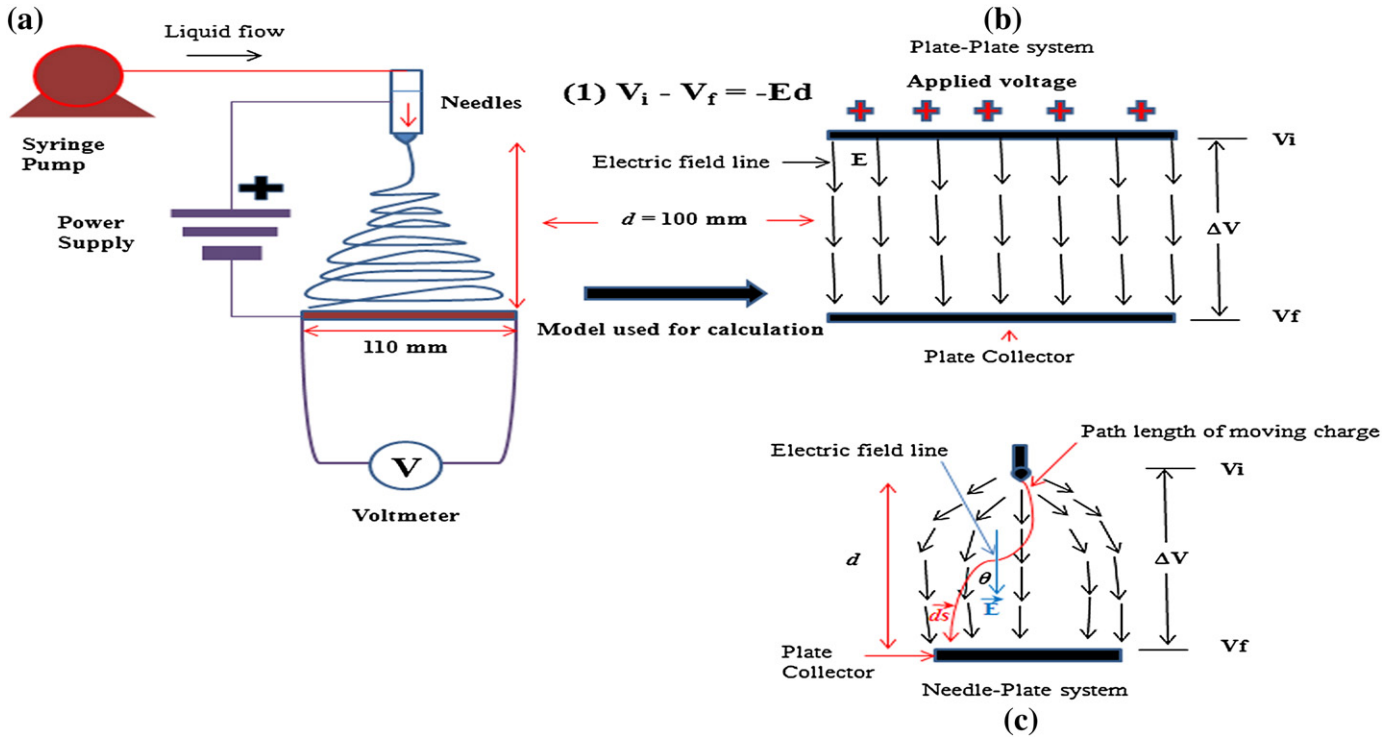

Fig. 11. A schematic diagram of (a) the electrospinning setup for both needle types for the calculation of electric field difference between the needle tip and the grounded collector, (b) parallel plate conductor and the grounded collector, where E denotes the electrical field lines, ΔV is the change in voltage, d is the distance between needle tip and the grounded collector, V_i is the voltage generated by the power supply and V_f is the voltage measured by the voltmeter, and (c) needle–plate system where ds denotes the path length of moving charge and θ is the angle created with charge path deviation. The arrows above ds and E represent vector quantities.

and 15 kV, were calculated to be 50 V/mm, 100 V/mm and 150 V/mm, respectively. This method is not accurate either since it does not take into account any of the aforementioned parameters, such as needle geometry, and there is no way to discern between the differences in the electric field generation for both needle setups.

Therefore, using the parallel method is not suitable to study electrical field generation during electrospinning. In addition to the aforementioned parameters, there were other vital factors which were also not taken into account using this method. Among these are the electrical field angle deviation from the needle tip to the collector, the permittivity of the medium between the aforementioned "plates" and the gap between the needles (Fig. 1b). Since this was not the case, the following model could be used to better understand the electrical field generation between the two needle setups.

This model can be applied to more general and relevant cases where the electric field and its direction can be changing, the expression must be generalised to a line integral, where *ds* is the path length of the moving charge, E is the electrical field line and θ is the angle which is created as the charge moves from the needle towards the grounded collector (Fig. 11c):

$$V_i - V_f = -\int \vec{E} \cdot \vec{ds}. \quad (2)$$

This is the closest possible electric field line configuration to the actual electrospinning setup but experimentally it was not possible to measure deviation of the electric field that is present within our setup and therefore not used. A thorough investigation into electric field generation is still required to fully understand how it affects fibre generation during electrospinning. Computer simulations are still not close enough to reality and, as we have demonstrated, a more practical approach towards understanding the electric field is also not accurate either. However, combination of both methods, i.e. computer simulation and experimental measurements and taking into account the factors such as needle geometry, may generate results which could give a more precise understanding of the difference in electric field especially when needles of different conductivity are used to electrospin fibres.

3.6. Application of glass needle

Electrospinning with a glass needle may not have credible apparent benefits over the conventional steel needle as yet but there is a potential for more exploration in this area. One of the main problems with small diameter steel needles is blockages due to accumulation of solvent/polymer residue which requires constant cleaning. With a glass needle, needle re-use can be eliminated due to their low manufacturing cost per needle (up to ×8 cheaper) when compared to their steel needle counterparts. Furthermore, understanding its utility in multiple needle setups could prove useful in the industry where cost is the driving force behind novel research. In addition, glass overcomes many problems associated with steel corrosion by being more resistant to chemical attack.

Conversely, needleless electrospinning (Niu, Wang, & Lin, 2012) has been shown to overcome many of the problems associated with conventional needle based electrospinning but, unlike multiple needle setups, it does not benefit from the co-flowing liquids to form core-sheath structures. Furthermore, the jet initiation voltage is much higher (>40 kV) compared to the glass–needle setup we presented in our study.

Overall, glass–steel needle electrospinning is not, at present, fully understood and developed but could be seen as a potential intermediate setup between steel needle and needleless electrospinning setups to produce fibres.

4. Conclusions

Electrospinning using a combination of a glass and a steel needle was successfully carried out for the first time using ethyl cellulose as the processed material. A thorough comparison was made with a steel–steel needle electrospinning setup with regard to fibre aspect ratio and the influence of applied voltage thereon. Introduction of the glass needle to the electrospinning setup resulted in thinner fibres with increasing applied voltage whereas the reverse was true when only steel needles were employed to form the fibres. The analysis of the electric field generation during electrospinning illustrated the need to take into consideration many other factors (such as needle geometry) associated with the entire fibre forming process in order to fully understand the electric field and its effects on fibre generation and to move away from computer simulated models. All the results indicate that glass–steel needle electrospinning setup can generate fibres with smaller diameters compared with steel–steel needle electrospinning setup.

Acknowledgements

The authors would like to thank Unilever and the EPSRC (doctoral research program of Bilal Ahmad) for providing the funding for this work via an industrial case studentship. The authors would also like to thank the Archaeology Department at UCL for the use of their scanning electron microscopes in this study and the Engineering Instrument Loan Pool for lending us the Phantom V7.1 high speed camera, especially Mr. Adrian Walker for his generous help.

References

Ahmad, B., Gunduz, O., Stoyanov, S., Pelan, E., Stride, E., & Edirisinghe, M. J. (2012). A novel hybrid system for the fabrication of a fibrous mesh with micro-inclusions. *Carbohydrate Polymers*, *89*, 222–229.

Ahmad, B., Stride, E., & Edirisinghe, M. J. (2012). Calcium alginate foams prepared by a microfluidic T-junction system: Stability and food applications. *Food and Bioprocess Technology*, *5*, 2848–2857.

Angammana, C. J., & Jayaram, S. H. (2011). The effects of electric field on the multijet electrospinning process and fiber morphology. *IEEE Transactions on Industry Applications*, *47*, 1028–1035.

Chang, S. -T., Chen, L. -C., Lin, S. -B., & Chen, H. -H. (2012). Nano-biomaterials application: Morphology and physical properties of bacterial cellulose/gelatin composites via crosslinking. *Food Hydrocolloids*, *27*, 137–144.

Cuculo, J. A., Aminuddin, N., & Frey, M. W. (2000). Solvent spun cellulose fibers. In D. R. Salem (Ed.), *Structure formation in polymeric fibers* (pp. 296–328). Munich: Hanser Publishers.

Dosunmu, O. O., Chase, G. G., Kataphinan, W., & Reneker, D. H. (2006). Electrospinning of polymer nanofibres from multiple jets on a porous tubular surface. *Nanotechnology*, *17*, 1123–1127.

Dzenis, Y. (2004). Spinning continuous fibers for nanotechnology. *Science*, *304*, 1917–1919.

Hohman, M. M., Shin, M., Rutledge, G., & Brenner, M. P. (2001). Electrospinning and electrically forced jets. I. Stability theory. *Physics of Fluids*, *13*, 2201–2220.

Jaworek, A., & Krupa, A. (1992). Morphological studies of electrodynamic spraying of water. *Transactions in Institute of Fluid-Flow Machinery*, *94*, 155–172.

Jimenez, M., Garcia, H. S., & Beristain, C. I. (2004). Spray-drying microencapsulation and oxidative stability of conjugated linoleic acid. *European Food Research and Technology*, *219*, 588–592.

Kim, C. -W., Kim, D. -S., Kang, S. -Y., Marquez, M., & Joo, Y. L. (2006). Structural studies of electrospun cellulose nanofibers. *Polymer*, *47*, 5097–5107.

Kim, S. J., Lee, C. K., & Kim, S. I. (2005). Effect of ionic salts on the processing of poly(2-acrylamido-2-methyl-1-propane sulfonic acid) nanofibers. *Journal of Applied Polymer Science*, *96*, 1388–1393.

Kris-Etherton, P.M., Hecker, K. D., Bonanome, A., Coval, S. M., Binkoski, A. E., Hilpert, K. F., et al. (2002). Bioactive compounds in foods: Their role in the prevention of cardiovascular disease and cancer. *The American Journal of Medicine*, *113*, 71S–88S.

Lee, J. S., Choi, K. H., Ghim, H. D., Kim, S. S., Chun, D. H., Kim, H. Y., et al. (2004). Role of molecular weight of atactic poly(vinyl alcohol) (PVA) in the structure and properties of PVA nanofabric prepared by electrospinning. *Journal of Applied Polymer Science*, *93*, 1638–1646.

Li, D., & Xia, Y. (2004). Electrospinning of nanofibers: Reinventing the wheel? *Advanced Materials*, *16*, 1151–1170.

Liu, R. H. (2003). Health benefits of fruit and vegetables are from additive and synergistic combinations of phytochemicals. *The American Journal of Clinical Nutrition*, *78*, 517S–520S.

Lopez-Rubio, A., Gavara, R., & Lagaron, J. A. (2006). Bioactive packaging: Turning foods into healthier foods through biomaterials. *Trends in Food Science & Technology*, *17*, 567–575.

Mo, X. M., Xu, C. Y., Kotaki, M., & Ramakrishna, S. (2004). Electrospun P(LLA-CL) nanofiber: A biomimetic extracellular matrix for smooth muscle cell and endothelial cell proliferation. *Biomaterials*, *25*, 1883–1890.

Niu, H., Wang, X., & Lin, T. (2012). Upward needless electrospinning of nanofibres. *Journal of Engineering Fibre and Fabric*, *7*, 7–22.

Ramakrishna, S., Fujihara, K., Teo, W. -E., & Ma, Z. (2005). *An introduction to electrospinning and nanofibers*. Hackensack, NJ; London: World Scientific.

Reneker, D. H., Yarin, A. L., Fong, H., & Koombhongse, S. (2000). Bending instability of electrically charged liquid jets of polymer solutions in electrospinning. *Journal of Applied Physics*, *87*, 4531–4547.

Shin, Y. M., Hohman, M. M., Brenner, M. P., & Rutledge, G. C. (2001). Experimental characterization of electrospinning: The electrically forced jet and instabilities. *Polymer*, *42*, 09955–09967.

Sill, T. J., & von Recum, H. A. (2008). Electrospinning: Applications in drug delivery and tissue engineering. *Biomaterials*, *29*, 1989–2006.

Tang, K., & Gomez, A. (1995). Generation of monodisperse water droplets from electrosprays in a corona-assisted cone-jet mode. *Journal of Colloid and Interface Science*, *175*, 326–332.

Ting, Si, Li, G. -B., Chen, X. -X., Tian, R. -J., & Yin, X. -Z. (2012). Experimental investigation on flow modes of electrospinning. *Acta Mechanica Sinica*, *28*, 644–652.

Yan, Z., Chen, S., Wang, H., Wang, B., Wang, C., & Jiang, J. (2008). Cellulose synthesised by *Acetobacter xylinum* in the presence of multi-walled carbon nanotubes. *Carbohydrate Research*, *343*, 73–80.

Yarin, A. L. (2011). Coaxial electrospinning and emulsion electrospinning of core–shell fibers. *Polymers for Advanced Technologies*, *22*, 310–317.

Ying, Y., Zhidong, J., Qiang, L., Lei, H., Haifeng, G., Liming, W., et al. (2006). Multiple jets in electrospinning. *Paper presented at the 8th International Conference on Properties and Applications of Dielectric Materials, Bali.* : IEEE.

Yu, J. H., Fridrikh, S. V., & Rutledge, G. C. (2004). Production of submicrometer diameter fibers by two-fluid electrospinning. *Advanced Materials*, *16*, 1562–1566.

Zhang, S. (2003). Fabrication of novel biomaterials through molecular self-assembly. *Nature Biotechnology*, *21*, 1171–1178.

Zhang, J. -F., Yang, D. -Z., Xu, F., Zhang, Z. -P., Yin, R. -X., & Nie, J. (2009). Electrospun core–shell structure nanofibers from homogeneous solution of poly(ethylene oxide)/chitosan. *Macromolecules*, *42*, 5278–5284.